JOURNAL OF CATALYSIS 74, 373–381 (1982)

Sulfonated Poly(styrene-divinylbenzene) Catalysts

III. The Influence of Polymer Physical Properties on the Kinetics of Methanol Dehydration

R. B. DIEMER, JR.,[1] K. M. DOOLEY, B. C. GATES,[2] AND R. L. ALBRIGHT*

*Center for Catalytic Science and Technology, Department of Chemical Engineering, University of Delaware, Newark, Delaware 19711, and *Rohm and Haas Company, Philadelphia, Pennsylvania 19105*

Received July 16, 1981; revised December 7, 1981

Kinetics of methanol dehydration catalyzed by sulfonated macroporous poly(styrene-divinylbenzene) was measured with a packed bed flow reactor operated at 1 atm and 77–107°C. Data were obtained for a set of catalysts with systematically varied crosslinking, average macropore diameter, and surface area. The results demonstrate that swelling and diffusion effects were negligible. A single form of Langmuir–Hinshelwood rate equation represents the data for all the macroporous catalysts and also a gel-form catalyst. Comparison of intrinsic rate constants showed that surface sites are less active than sites in the polymer gel interior.

INTRODUCTION

Macroporous ion-exchange resins can be prepared with a wide range of physical properties, allowing control of the swellability of the polymer matrix, the rates of reactant and product transport, and the intrinsic catalytic activity. The macroporous resins consist of agglomerates of nearly spherical microparticles of gelular polymer, separated by macropores. In an accompanying article (*1*), we reported characterization of a series of macroporous sulfonic acid resins for catalysis of the reesterification reaction of ethyl acetate with *n*-propanol. The data were represented by a model accounting for diffusion in macropores, Langmuir adsorption on microparticle surfaces, diffusion/swelling in microparticles, and reaction in the microparticles.

In this work, complementing that mentioned above, the goal was to consider the influence of polymer physical properties on the intrinsic catalytic activity of a macroporous sulfonic acid resin. Methanol was chosen as the reactant because it is a small, polar molecule expected to swell the polymer effectively, possibly allowing catalysis to occur in the absence of significant intraparticle concentration gradients. Kinetics of the methanol dehydration was measured with a set of catalysts having systematically varied physical properties (crosslinking, average macropore diameter, and surface area) to allow an assessment of the diffusion and swelling influence (*2*). The conditions of the catalytic reaction experiments were chosen to be similar to those of researchers who had previously characterized gel-form ("microporous") sulfonic acid resins (*3, 4*) and macroporous resins (*5*); a specific goal was to compare the intrinsic catalytic activities of our resins to theirs, and explain the difference in terms of the polymer physical properties.

EXPERIMENTAL

Materials. The catalysts were sulfonated, macroporous copolymers of styrene, divinylbenzene, and ethylvinylbenzene, the properties of which are given in Table 1 of the accompanying article (*1*). Certified ACS reagent grade methanol was supplied by Fisher, and industrial grade helium (~15

[1] Present address: E. I. du Pont de Nemours and Co., Belle, W.V. 25015.

[2] To whom correspondence should be addressed.

0021-9517/82/040373-09$02.00/0

ppm H_2O, 99.995% pure) was supplied by Linde.

Apparatus. Initial reaction rate data for the reaction of methanol to give dimethyl ether and water were determined with a thermostated, packed-bed flow reactor, interfaced to the sampling valve of a gas chromatograph (GLC). Differential conversions were determined for pure methanol, methanol–water, and methanol–helium feeds at atmospheric pressure and 77–107°C. These mixtures were vaporized and mixed in a 20-cm-long by 1.25-cm-o.d. heated vertical stainless-steel tube packed with 3-mm-diameter glass beads.

The reactor was a vertical (downflow) stainless-steel tube, 2.5 cm in i.d. and 41 cm long, encased in an electric furnace with a temperature control loop. The catalyst bed length was approximately 1 cm, and a thermocouple probe extended down to within 2 cm of the top of the bed. This probe temperature was controlled with a precision of ±0.5°C.

The reactor exit tube and the gas sampling valve were heated to prevent condensation of product vapors. The GLC column was a 2-mm-i.d., 2-m-long glass column containing Porapak P (80/100 mesh) and temperature programmed with a 2-min initial hold at 75°C followed by a 20°C/min ramp to 155°C. A flame ionization detector was used.

Procedure. Liquid feed mixtures were metered with a syringe pump. Helium flow rate was measured with a soap film flow meter. Conversions were calculated from dimethyl ether-to-methanol chromatographic peak area ratios. Water was not detected. Repeated analyses (usually four) were obtained at steady state for each experimental condition. Periodic conversion checks confirmed the absence of catalyst deactivation.

Evaluation and errors. Rates of dimethyl ether formation were calculated from differential conversions and feed flow rates. No side reactions were observed. Experimental error in GLC analyses and flow rate data indicated that the reported reaction rates are precise to within ±10%, except for data obtained with feeds containing >40 mole% water or data obtained at temperatures <80°C. Details of the apparatus and procedures are given elsewhere (*6*).

RESULTS AND DISCUSSION

The observed rates of methanol dehydration catalyzed by the macroporous resins are shown in Fig. 1. The activities of the various catalysts are similar, suggesting that the resins were completely swollen with reactant and that transport processes did not significantly influence the rates.

The rate data for all four catalysts (obtained with pure methanol feed) are collected in an Arrhenius plot (Fig. 2) where they are compared with literature data (*4, 5*). The catalytic activities of our polymers are less than those of the polymer catalysts of previous studies, indicating that methanol dehydration rates can be influenced by large changes in the physical properties of the polymer catalysts.

We proceed to analyze the catalytic reaction rate data, first establishing that transport effects are not significant for our resins. The analysis is built upon the model for swellable micro/macropore catalysts developed in the accompanying article (*1*). Details of some of the following calculations are given elsewhere (*6*) along with calculations (by standard methods) demonstrating the absence of signficant temperature gradients and of concentration gradients external to the catalyst particles.

Earlier experiments with methanol dehydration catalyzed by gel-form sulfonic acid resins and membranes (*3, 4, 7*) demonstrated the absence of an effect of catalyst particle size on rate—and therefore the absence of significant resistances to transport of reactants and products in the polymer matrix. The results of the reported experiments are consistent with a Langmuir–Hinshelwood model, whereby the rate-determining step is the reaction of two methanol molecules hydrogen-bonded to neighboring

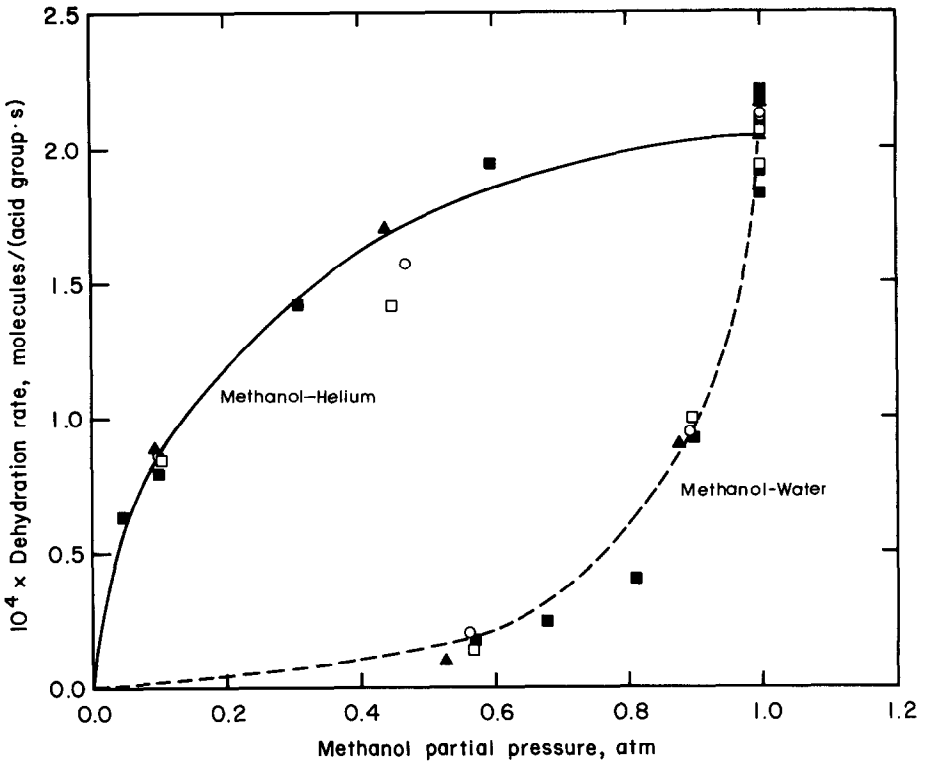

FIG. 1. Initial rates of methanol dehydration catalyzed by macroporous sulfonic acid resins. The upper curve is for methanol–helium mixtures, and the lower curve is for methanol–water mixtures. The curves are the fits to the data given by Eq. (21) with the regression parameters of Table 4. The experimental values are: ○, catalyst A; ▲, catalyst B; ■, catalyst C; □, catalyst D.

$-SO_3H$ groups present in a hydrogen-bonded network of $-SO_3H$ groups; water is a reaction inhibitor (*3*, *4*, *7*).

Using these results as a basis, we represent the intrinsic kinetics as second-order in chemisorbed methanol and apply the model developed earlier (*1*) to account for the effects of swelling and transport. The relevant equations are the following [with the nomenclature given previously (*1*), and the new subscripts m, w, and e denoting methanol, water, and ether, respectively]:

$$r_{\mu\text{obs}} = \frac{\left[2\int_{C_\mu^0}^{C_\mu^s} kDC_\mu^2\left(\frac{\epsilon_\mu}{2-\epsilon_\mu}\right)^2 dC_\mu\right]^{1/2}}{\left(\frac{d_\mu^0}{6}\right)(1-\epsilon_\mu^s)^{-1/2}} \quad (1)$$

$$\epsilon_\mu^s = \bar{v}_m C_{\mu m}^s + \bar{v}_w C_{\mu w}^s + \bar{v}_e C_{\mu e}^s. \quad (2)$$

$$\epsilon_\mu = \bar{v}_m C_{\mu m} + \bar{v}_w C_{\mu w} + \bar{v}_e C_{\mu e}. \quad (3)$$

$$C_{\mu m}^s = \theta\rho_\mu^0(1-\epsilon_\mu^s) \times \left(\frac{K_m P_m}{1 + K_m P_m + K_w P_w}\right). \quad (4)$$

TABLE 1A

Calculated Reaction Rate Ratio—Catalysts C and D[a]

Case	$(r_{\text{obs}})_C/(r_{\text{obs}})_D$
I	1.0
II	1.4–1.7
III	1.4–1.7 $(f_C/f_D)^{1/2}$
IV	0.89

[a] Note: $f = \int_{C_M^0}^{C_M^s} (1-\epsilon_\mu^s)^{1/2}\left(\int_{C_\mu^0}^{C_\mu^s} kDC_\mu^2\left(\frac{\epsilon_\mu}{2-\epsilon_\mu}\right)^2 dC_\mu\right)^{1/2} dC.$

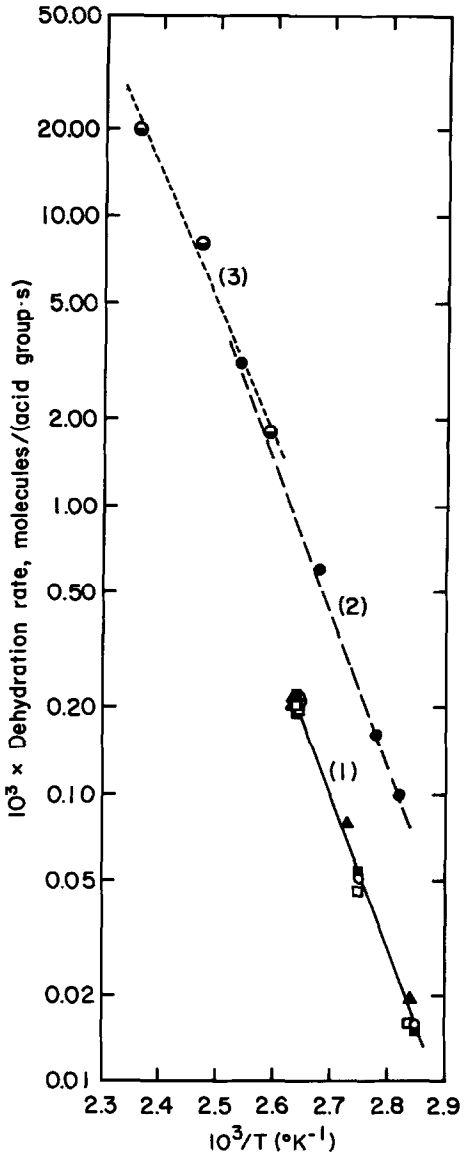

FIG. 2. Arrhenius plots: comparison of activities of sulfonic acid resin catalysts for methanol dehydration. The rates were determined at a methanol partial pressure of 1 atm. The lines were obtained by linear regression of the experimental values. (1) This work, (2) Gates and Johanson (*4*), (3) Thanh *et al.* (*5*).

In Eq. (1), the integral is over reactant concentration in the microparticles, and $r_{\mu obs}$ is the rate that would be observed just outside a microparticle; the rate is given per unit volume of microparticle. The observed rate in moles/(equiv. of $-SO_3H$ groups · s) is found by taking into account the contributions of all the microparticles from the macroparticle center to its surface:

$$r_{obs} = \frac{\eta_M R(C_M^s)}{\theta \rho_M} = \frac{\left[2 \int_{C_M^0}^{C_M^s} D'_M(C) R(C) dC\right]^{1/2}}{\theta \rho_M (d_M/6)}. \quad (5)$$

$$R(C) = r_{\mu obs}(1 - \epsilon_M). \quad (6)$$

The rate per $-SO_3H$ group is preferred because there are differences in the $-SO_3H$ group contents of the various catalysts (*1*, *4*, *5*).

Our macroporous catalysts have been prepared with systematic variations in physical properties, and we evaluate the effects of these variations one at a time by selecting appropriate pairs of catalysts. For example, catalysts C and D have similar microparticle properties but different macropore diameters (Ref. *1*, Table 1). We recognize four classes of transport limitations in the macropores and microparticles, denoting each with a Roman numeral:

(I) There are no appreciable macropore or microparticle concentration gradients in either catalyst.

(II) Gradients of each type are appreciable in both catalysts.

(III) Gradients of each type are significant in D, with only microparticle gradients significant in C.

(IV) Only microparticle gradients are significant in either catalyst.

For these four cases, the respective ratios of the observed rates of methanol dehydration for the two catalysts, namely $(r_{obs})_C/(r_{obs})_D$, can be evaluated by means of Eqs. (1), (5), and (6). For case I this ratio reduces to unity; in the other cases, the equations can be simplified, and the ratios expressed as follows:

$$\text{Case II: } \frac{(r_{obs})_C}{(r_{obs})_D} = \frac{(F_{II})_C}{(F_{II})_D} \quad (7)$$

$$\text{Case III: } \frac{(r_{obs})_C}{(r_{obs})_D} = \frac{(F_{III})_C}{(F_{III})_D} \tag{8}$$

$$\text{Case IV: } \frac{(r_{obs})_C}{(r_{obs})_D} = \frac{(F_{IV})_C}{(F_{IV})_D} \tag{9}$$

where

$$F_{II} = [\bar{D}^{1/2}\epsilon_M(1 - \epsilon_M)^{1/2}/\theta\rho_M d_\mu^{01/2}] \tag{10}$$

$$F_{III} = [\bar{D}^{1/2}\epsilon_M(1 - \epsilon_M)^{1/2}/\theta\rho_M d_\mu^{01/2}] \times \left[\int_{C_M^0}^{C_M^s} (1 - \epsilon_\mu^s)^{1/2} \times \left(\int_{C_\mu^0}^{C_\mu^s} kDC_\mu^2 \times \left(\frac{\epsilon_\mu}{2 - \epsilon_\mu}\right)^2 dC_\mu\right)^{1/2} dC\right]^{1/2} \tag{11}$$

$$F_{IV} = [(1 - \epsilon_M)/\theta\rho_M d_\mu^0]. \tag{12}$$

The diffusivities of reactants in the macropores are independent of reactant concentration (*6*), and therefore the ratios of observed rates are approximately independent of concentration.

For each case, the ratios of rates were evaluated using estimates of the physical properties, and the results are collected in Table 1A. The unknown factor $(f_C/f_D)^{1/2}$ for case III in Table 1A is estimated to lie between 0.7 and 1. The observed ratios of rates for the catalyst pair are summarized in Table 1B; comparison of the calculated and observed ratios confirms that significant macropore concentration gradients are absent, although the result from case IV suggests the possibility that appreciable microparticle gradients may exist.

TABLE 1B

Observed Reaction Rate Ratio—Catalysts C and D

T (°C)	p_m (atm)	p_w (atm)	$(r_{obs})_C/(r_{obs})_D$
106	1.00	—	1.01 ± 0.07
90	1.00	—	1.17 ± 0.17
78	1.00	—	0.89 ± 0.20
106	0.10	—	0.94 ± 0.16
106	0.90	0.10	0.92 ± 0.11
106	0.57	0.43	0.86 ± 0.29

These conclusions apply to the other catalysts as well, since they have similar activities and similar macropore structures. We now proceed using the simplification that macropore gradients are negligible.

The catalyst pair A and C is appropriate for diagnosing the influence of microparticle surface area on catalytic activity, since these two catalysts are similar in all but this property. An effect of surface area on activity might be an indication of differences in activity of surface acid groups compared with those in the microparticle interior.

Again we recognize four classes of catalyst behavior:

(I) There are no significant microparticle concentration gradients or effects of surface area.

(II) There are significant effects of surface area but no microparticle gradients.

(III) Microparticle concentration gradients and the effects of surface area are appreciable.

(IV) There are no effects of surface area, but there are significant microparticle concentration gradients.

In evaluating the ratios of rates associated with these four cases, we need to estimate partial molar volumes and adsorption equilibrium coefficients to calculate surface adsorbate concentrations. The correct values were bracketed using the limiting cases: (1) as $K_i \to 0$, $\bar{v} \to \bar{v}_{\text{saturated liquid}}$ and (2) as $K_i \to \infty$, $\bar{v} \to \bar{v}_{max}$, as calculated from the resin hydration data of Lal and Douglas (*8*). The rate ratios $(r_{obs})_A/(r_{obs})_C$ for the four cases can then be found by application of Eqs. (1)–(4). For case I these equations result in a ratio of rates equal to unity; for the other cases the results are:

$$\text{Case II: } \frac{(r_{obs})_A}{(r_{obs})_C} = \frac{(F_{II})_A}{(F_{II})_C} \tag{13}$$

$$\text{Case III: } \frac{(r_{obs})_A}{(r_{obs})_C} = \frac{(F_{III})_A}{(F_{III})_C} \tag{14}$$

$$\text{Case IV: } \frac{(r_{obs})_A}{(r_{obs})_C} = \frac{(F_{IV})_A}{(F_{IV})_C} \tag{15}$$

where

$$F_{II} = [D(C_\mu^s)^{1/2}k^{1/2}C_\mu^s\epsilon_\mu^s(1 - \epsilon_\mu^s)^{1/2}/(2 - \epsilon_\mu^s)d_\mu^0\theta\rho_\mu^0] \quad (16)$$

$$F_{III} = [\bar{D}^{1/2}k^{1/2}C_\mu^{s3/2}\epsilon_\mu^s(1 - \epsilon_\mu^s)^{1/2}/(2 - \epsilon_\mu^s)d_\mu^0\theta\rho_\mu^0] \quad (17)$$

$$F_{IV} = [(d_\mu^0\theta\rho_\mu^0)^{-1}]. \quad (18)$$

These ratios were evaluated, and the results of the calculations appear in Table 2A. For cases II and III the ratios $(k_A/k_C)^{1/2}$ may not be unity because of the expected involvement of more than one $-SO_3H$ group per catalytic site (*3, 4, 7*). For the lower surface-area catalyst C, with a larger percentage of $-SO_3H$ groups in the microparticle gel interiors, it is expected that the number of $-SO_3H$ groups available for hydrogen bonding is greater, meaning a greater number of ensembles of $-SO_3H$ groups, and therefore a larger intrinsic rate constant for C, and ratios of rate constants for cases II and III slightly less than unity. In any event, it is evident from a comparison of the calculated and observed ratios of rates (Tables 2A and 2B) that the effects of internal microparticle surface area on catalytic activity are negligible and that microparticle concentration gradients may be neglected in these lightly crosslinked catalysts.

To determine the influence of microparticle crosslinking for more highly crosslinked polymers, we compare catalysts A and B, which are 8 and 16% crosslinked, respectively. There are two remaining classes of transport behavior to be considered.

TABLE 2A

Calculated Reaction Rate Ratio at 106°C—Catalysts A and C

Case	$(r_{obs})_A/(r_{obs})_C$
I	1.0
II	(5.0–12) $[k_A/k_C]^{1/2}$
III	(7.6–18) $[k_A/k_C]^{1/2}$
IV	2.2

TABLE 2B

Observed Reaction Rate Ratio—Catalysts A and C

T (°C)	p_m (atm)	p_w (atm)	$(r_{obs})_A/(r_{obs})_C$
106	1.00	—	1.05 ± 0.06
91	1.00	—	0.93 ± 0.13
78	1.00	—	1.14 ± 0.13
106	0.10	—	1.08 ± 0.15
106	0.90	0.10	1.02 ± 0.12
106	0.57	0.43	1.70 ± 0.98

(I) Crosslinking has no effect on activity.

(II) There are significant microparticle concentration gradients for the more highly crosslinked catalyst.

The ratios of the rates again have been found by application of Eqs. (1)–(4) using the limiting values for $\bar{v}$ and K_i mentioned above. The ratio of rates for case I reduces to unity and for case II it is approximated as

$$\text{Case II: } \frac{(r_{obs})_A}{(r_{obs})_B} = \frac{(2)(F_{II})_A}{(F_{II})_B} \quad (19)$$

where

$$F_{II} = [(D(C_\mu^s))^{1/2}k^{1/2}C_\mu^s\epsilon_\mu^s(1 - \epsilon_\mu^s)^{1/2}/(2 - \epsilon_\mu^s)d_\mu^0\theta\rho_\mu^0](C_\mu^s - C_\mu^0)^{1/2}. \quad (20)$$

The ratios were evaluated and the results appear in Table 3A. The unknown factor $(f_A/f_B)^{1/2}$ for case II in Table 3 is estimated to lie between 0.7 and 1.0. The ratio of the rate constants $(k_A/k_B)^{1/2}$ may not be unity because of possible differences in the structures of catalytic sites in catalysts of different crosslinkings. In the accompanying article (Ref. *1*, Table 4) it was shown that

TABLE 3A

Calculated Reaction Rate Ratio at 106°C—Catalysts A and B[a]

Case	$(r_{obs})_A/(r_{obs})_B$
I	1.0
II	(2.3–2.4) $(k_A/k_B)^{1/2}(f_A/f_B)^{1/2}$

[a] Note: $f = (C_\mu^s - C_\mu^0)$.

TABLE 3B

Observed Reaction Rate Ratio—Catalysts A and B

T (°C)	p_m (atm)	p_w (atm)	$(r_{obs})_A/(r_{obs})_B$
106	1.00	—	1.00 ± 0.08
106	0.45	—	0.92 ± 0.11
106	0.10	—	0.96 ± 0.12
92	1.00	—	0.63 ± 0.06
78	1.00	—	0.90 ± 0.15
106	0.90	0.10	1.06 ± 0.12
106	0.55	0.45	2.09 ± 1.13

these differences could result in a higher intrinsic rate constant for the more highly crosslinked catalyst and therefore in a ratio of rates for case II closer to unity. With this result, after comparison of calculated and observed ratios of rates we find it impossible to judge whether appreciable resistances to transport exist in the microparticles of catalyst B.

If we assume that there were no significant resistances and therefore that intrinsic kinetics was observed, then a single rate expression should correlate all kinetics data for all the catalysts. If the data for catalyst B do not fit this expression, then it can be concluded that significant microparticle concentration gradients were present in this catalyst.

Therefore, a number of Langmuir–Hinshelwood rate expressions were compared with the kinetics data for each catalyst using nonlinear regression techniques (*9*). Three rate equations, statistically indistinguishable, emerged as best fitting all the data:

$$r = k\left(\frac{K_m P_m}{1 + K_m P_m + K_w p_w}\right)^2 \qquad (21)$$

$$r = \frac{k\,K_m P_m}{(1 + (K_m P_m)^{1/2} + K_w P_w)^2} \qquad (22)$$

$$r = \frac{k\,K_m P_m}{(1 + K_m P_m + K_w P_w)} \quad . \qquad (23)$$

[The units of r are mol/(equiv · s).] Fig. 1 shows the fit of Eq. (21) (other fits are almost indistinguishable) to data obtained at 106°C and 1 atm. Two curves are shown, one for methanol–helium mixtures and one for methanol–water mixtures. Since all the data are adequately described by the same rate expressions, we infer that microparticle diffusion effects are negligible for even the most highly crosslinked catalyst.

Literature data obtained with an 8%-crosslinked gel-form resin at 119°C were fitted to Eq. (21) (*3*, *4*), whereas data obtained for a macroporous polymer at 150°C were fitted to Eq. (22) (*5*). The temperature 106°C was chosen for comparison of the

TABLE 4

Comparison of Rate Equations and Parameters with Literature Data

	This work	Gates and Johanson (*4*)	Thanh *et al.* (*5*)
Pressure (atm)	1	1	1
Temperature range (°C)	77–106	80–120	111–150
Eq. (21) Parameters at 106°C			
k (mol/s · equiv)	$(2.3 \pm 0.1) \times 10^{-4}$	9.4×10^{-4}	3.1×10^{-4}
K_m (atm^{-1})	15 ± 3	1	18
K_w (atm^{-1})	63 ± 15	11	Not measured
Eq. (22) Parameters at 106°C			
k (mol/s · equiv)	$(3.7 \pm 0.4) \times 10^{-4}$	—[a]	4.5×10^{-4}
K_m (atm^{-1})	8.6 ± 3.0	—[a]	15
K_w (atm^{-1})	17 ± 3	—[a]	Not measured

[a] No fit found.

present data to these literature data, and the equation parameters were obtained as follows. For the data of Thanh *et al.* (*5*), parameters were extrapolated using the Arrhenius and van't Hoff equations. The paper by Gates and Johanson (*4*) provided estimates of K_m and K_w over the range 100–120°C, and interpolation with the van't Hoff equation yielded estimates for 106°C. An Arrhenius plot of their data (Fig. 2) gave an apparent activation energy of 24.4 kcal/mole. This value was used to adjust the Gates and Johanson rate constant to 106°C; the value is in excellent agreement with the result obtained in this work (Fig. 2), 23.9 ± 0.7 kcal/mole.

To compare all the data using both Eqs. (21) and (22), the rate parameters for one equation were used to generate rate-partial pressure values, which were then fitted to the other equation. For example, the Thanh *et al.* parameters for Eq. (22) were used to generate rate-partial pressure values subsequently fit to Eq. (21). It was found that the values of Gates and Johanson generated in this manner from Eq. (21) could not be fit adequately to Eq. (22).

A summary of the resulting rate equations is given in Table 4. The comparison shows that the results of the present work and that of Thanh *et al.* (who also used a macroporous catalyst) are in rough agreement, as indicated by all the parameter values, but these differ markedly from the results of Gates and Johanson, who used a gel-form catalyst.

The properties of the catalysts used by the three sets of investigators are compared in Table 5; they suggest an explanation for the observed rate differences. In the present work and that of Thanh *et al.*, the macroporous resins used had high surface areas and large fractions of the $-SO_3H$ groups present on surfaces; in contrast, the gelular resin of Gates and Johanson had virtually all of the acid groups present within the polymer gel. The constants K_m and K_w are larger for the macroporous resins than for the gel, suggesting that the polar molecules are preferentially associated with surface acid groups rather than those in the interior. On the other hand, the intrinsic rate constant is higher for the gelular resin; since both Eqs. (21) and (22) suggest rate-limiting reaction steps involving two adsorbed methanol molecules, we infer that the interior (gel-phase) $-SO_3H$ groups are more active because they have roughly

TABLE 5

Comparison of Key Resin Properties

	This work	Gates and Johanson (*4*)	Thanh *et al.* (*5*)
Microparticle density (g/cm^3)	1.41–1.50	1.45[a]	1.45[b]
Microparticle surface area (m^2/g)	11–24	0.083[c]	49
Crosslinking (wt% DVB)	8–16	8	25
Average microparticle diameter (Å)	1670–3870	5,000,000	840[c]
Concentration of acid groups (meq/g)	5.25–5.54	5.20	2.40
Fraction of $-SO_3H$ groups on microparticle surfaces	0.0068–0.0146	5.3×10^{-6}	0.0678

[a] Assumed.
[b] Per Rodriguez and Setínek (*10*).
[c] Calculated.

twice as many neighbors as surface sites, i.e., because the ensembles of $-SO_3H$ groups are more numerous. This suggestion is consistent with earlier suggestions of the effectiveness of ensembles of hydrogen-bonded $-SO_3H$ groups as catalytic sites (*3, 7*).

The fact that the data for the gelular resin did not fit Eq. (22), whereas the macroporous resin data fit both Eqs. (21) and (22), suggests that (21) is the more fundamentally correct form and that Eq. (22) represents a composite of surface and interior effects that should not be interpreted mechanistically within the Langmuir–Hinshelwood theory.

When Langmuir–Hinshelwood models are applied to account for catalysis by macroporous polymers, the adsorption equilibrium constants should be recognized as accounting both for surface adsorption and microparticle swelling equilibria. High-surface-area macroporous catalysts are desirable when there are significant transport resistances within the microparticles [e.g., when the reactants are hydrocarbons, which swell the polymer only slightly (*11*)]; but the present results show that they are not advantageous when the interior sites are more active than those on the surfaces; i.e., when ensembles of $-SO_3H$ groups constitute the catalytic sites.

ACKNOWLEDGMENT

We thank Rohm and Haas Company for support of the research.

REFERENCES

1. Dooley, K. M., Williams, J. A., Gates, B. C., and Albright, R. L., *J. Catal.* **74,** 361 (1982).
2. Albright, R. L., Dooley, K. M., and Gates, B. C., to be published.
3. Gates, B. C., and Johanson, L. N., *J. Catal.* **14,** 69 (1969).
4. Gates, B. C., and Johanson, L. N., *Amer. Inst. Chem. Eng. J.* **17,** 981 (1971).
5. Thanh, L. N., Setínek, K., and Beránek, L., *Coll. Czech. Chem. Commun.* **39,** 1253 (1974).
6. Diemer, R. B., Jr., M. Ch. E. Thesis, Univ. of Delaware, Newark, DE 1980.
7. Thornton, R., and Gates, B. C., *in* "Proceedings of the Fifth International Congress on Catalysis" (J. W. Hightower, Ed.), pp. 357–369. North Holland, Amsterdam, 1973.
8. Lal, B. B., and Douglas, W. J. M., *Ind. Eng. Chem. Fund.* **13,** 223 (1974).
9. Marquardt, D. W., *J. Soc. Ind. Appl. Math.* **2,** 431 (1963).
10. Rodriguez, O., and Setínek, K., *J. Catal.* **39,** 449 (1975).
11. Dooley, K. M., and Gates, B. C., to be published.